Journal of Materials Chemistry C

Accepted Manuscript

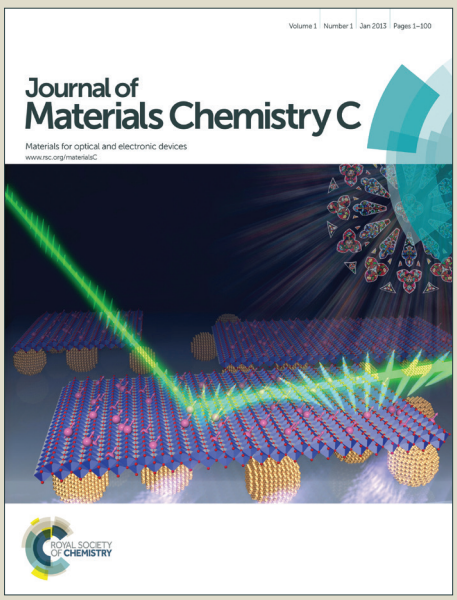

ROYAL SOCIETY OF CHEMISTRY

www.rsc.org/materialsC

Journal Name

ARTICLE

Enhanced thermoelectric performance through carrier scattering at heterojunction potentials in BiSbTe based composites with Cu_3SbSe_4 nanoinclusions

Received 00th January 20xx,
Accepted 00th January 20xx

DOI: 10.1039/x0xx00000x

www.rsc.org/

Yuanyue Li,[a] Di Li,[a] Xiaoying Qin*,[a] Xiuhui Yang,[b] Yongfei Liu,[a] Jian Zhang,[a] Yunchen Dou,[a] Chunjun Song[a] and Hongxing Xin[a]

*Corresponding author: xyqin@issp.ac.cn

Abstract

Thermoelectric materials with thermoelectric figure of merit, ZT, being much larger than unit at near room temperatures is vital for power generation by using low-grade waste heat. Here we show that by incorporating very small proportion (1 vol.%) of Cu_3SbSe_4 nanoparticles into BiSbTe matrix to form nanocomposites, besides large (~50%) reduction of lattice thermal conductivity, both enhanced thermopower through energy-dependent scattering and alleviated reduction of carrier mobility via carrier scattering at heterojunction potentials occur at elevated temperatures, which allow thermoelectric power factor of the composite material to reach ~37μW/(cm·K^2) at 467 K. Consequently, a largest value of ZT = 1.6 is achieved at 476 K. Moreover, it has excellent performance in broad temperature range (say, ZT=1.0 at 300 K and ZT=1.5 at 500 K), which makes this material attractive for cooling and power generation

1. Introduction

Thermoelectric (TE) materials can convert electrical power and heat energy reversely.[1] The efficiency of a TE material is evaluated by the thermoelectric figure of merit (ZT), expressed as $ZT = (S^2T)/\rho(\kappa_c + \kappa_L)$, where ρ, S, κ_c, κ_L and T are the electrical resistivity, Seebeck coefficient, carrier thermal conductivity, lattice thermal conductivity and absolute temperature, respectively.[2,3] Obviously, one can enhance ZT by maximizing power factor ($PF = S^2/\rho$) and/or minimizing total thermal conductivity ($\kappa = \kappa_c + \kappa_L$). Recent researches[4,5] indicate that nanostructuring or nanocompositing in bulk materials can dramatically reduce κ_L, but PF is seldom elevated simultaneously. Clearly, if one wants to obtain a ZT value much larger than unit, one has to elevate PF simultaneously. Previous studies showed that introduction of resonance distortion of electronic density of states (DOS) by doping to increase S can increase PF (such as in PbTe doped with Tl[2]), but no obvious reduction in κ_L was observed. Furthermore, an excellent alternative way to increase PF is to incorporate nanoinclusions into matrices to form nanocomposites in which energy filtering effect (EFE) would be enhanced through carrier scattering at the interface potentials, leading to increase in S.[6] But, in this case PF sometime declines due to large reduction in carrier mobility μ.[7,8] Hence, whether one can introduce in nanocomposites a proper heterojunction potentials that can not only bring about strong EFE but also give rise to increased μ_{in} (here μ_{in} is carrier mobility corresponding to carriers scattering at the interface potentials) and inhibit transport of minorities at elevated temperatures, in addition to enhancing phonon blocking, is greatly challenging, for this will result in large improvement of PF and ZT.

In present work, $Bi_{0.4}Sb_{1.6}Te_3$ (BiSbTe) based composites incorporated with nanophase Cu_3SbSe_4 was fabricated. BiSbTe alloys are the state-of-the-art thermoelectric materials at near room temperatures with a band gap of ~0.13-0.15eV.[9] Cu_3SbSe_4 is a p-type semiconductor with good thermoelectric performance at moderate temperatures and has a wider band gap of ~0.3-0.4eV.[10] Hence, as they contact each other, p-p type heterojunction potentials at the interfaces will form, which could bring about enhanced EFE and elevated μ_{in} at high temperatures. Indeed, Our results indicate that the incorporation of 1vol.% of Cu_3SbSe_4 results in ~5% increase in PF and ~50% decrease in κ_L at 467 K, leading to a largest ZT = 1.6. Moreover, the obtained material have high ZT (>1.4) in temperature range from 375 K to 500 K, which makes them suitable for cooling and low-grade waste-heat recovery applications.

2. Experimental

[a] Key Laboratory of Materials Physics, Institute of Solid State Physics, Chinese Academy of Science, 230031 Hefei, P. R. China.
[b] Department of Physics, Yulin Normal University, 537000 Yulin, People's Republic of China

Elemental Bi (99.99%, Alfa Aesar), Sb (99.5%, Sigma Aldrich), and Te (99.999%, Alfa Aesar) powders were weighted as starting materials. The powder mixture was loaded into quartz ampoule pumped under vacuum of 10^{-2} Pa and then heated to 1073 K for 10h. Then the ingot was grinded into powders. To prepare nanophase Cu_3SbSe_4 inclusions, 10 mmol $SbCl_3$ (99%, powder) and 40 mmol Se (99%, powder) and 400 mL ethylenediamine were put into a 800 mL glass beaker to react. After mixing uniformly, 30 mmol CuCl (99%, powder) was then put into the beaker. After about two hours, a large quantity of powders was precipitated. The solution was stirred by a magnetic stirrer at the speed of 1700 r/s maintaining a temperature of 150°C during the synthesis. After about two hours, a large quantity of powders was precipitated. The collected powder was filtered, washed with anhydrous ethanol and distilled water until a PH value close to 7, and then dried under vacuum at 60 °C for nearly 6h. The nanometer-sized Cu_3SbSe_4 and BiSbTe powders were mixed in a planetary mill for 2h in accordance with the volume ratios of 1:99, 2:98 and 3:97. Then the bulk nanocomposite samples were obtained by hot-pressing the blended powders under a pressure of 600 MPa in vacuum at 673 K for 1h.

The phase structure of the obtained samples was studied by X-ray diffraction (Philips diffractometer, Cu K_α radiation) at room temperature. The morphology and fractographs were observed by field emission scanning electron microscopy (FE-SEM). Electrical resistivity and Seebeck coefficient were measured by the ZEM-3 system from ULVAC under Helium atmosphere from 293 to 493 K. The thermal diffusivity D was measured using the laser flash method (Netzsch, LFA-457). It should be pointed out that due to the anisotropic characteristic of BiSbTe alloys, D is measured in the perpendicular direction to the pressing direction, ensuring that the thermal and electrical properties are measured in the same direction. The specific heat, C_p, was determined by differential scanning calorimetry (DSC Pyris Diamond). The density d was measured by the Archimedes' method. The resulting total thermal conductivity was calculated from the measured thermal diffusivity D, specific heat C_p, and density d according to the relationship $\kappa = DdC_p$. Hall coefficient was measured at 300 K by the Physical Property Measurement System (PPMS). The accuracies in measurements of resistivity, Seebeck coefficient and thermal conductivity are around ±2%, ±5% and ±5%, respectively. The uncertainty of ZT is around ±10%.

3. Results and discussions

The XRD patterns of BiSbTe, Cu_3SbSe_4 and $f(Cu_3SbSe_4)$/BiSbTe composite samples (f = 1, 2, and 3 vol.%) are shown in Figure 1. The main diffraction peaks correspond well to the standard JCPDS cards ($Bi_{0.5}Sb_{1.5}Te_3$: No. 72-1836, Cu_3SbSe_4: No. 85-0003), as shown in Figure 1 (curves (a) and (b)). Moreover, apart from the peaks of BiSbTe, there is an additional small peak at 2θ~27.3^o in patterns from (c) to (e), which corresponds to (112) peak of Cu_3SbSe_4, indicating that there are two phases BiSbTe and Cu_3SbSe_4 in the composite samples, no obvious impurity phase being detected. In addition, the average grain size for Cu_3SbSe_4 is 42 nm that is determined from peak broadening of the XRD pattern for Cu_3SbSe_4 (curve (b) in Figure1) based on Scherrer formula.

Figure 2**(a)** and **(b)** shows the FE-SEM images of BiSbTe (a) and Cu_3SbSe_4 (b) powders. One can observe that the average particle size of BiSbTe powders is around 500-1000nm, while the average particle size of Cu_3SbSe_4 powders is around 200nm. The fractographs of Cu_3SbSe_4/BiSbTe composite bulk samples are shown in Figure 2**(c)**. It can be seen from Figure 2**(c)** that some white spots with sizes of 40-60 nm distribute in the big gray grains (see the inset in Figure 2**(c)**). By careful inspection with energy dispersive X-ray spectroscopy (EDX), one finds that the areas with white spots contain element Cu (Figure 2**(d)**), indicating that the white spots are actually Cu_3SbSe_4 grains, in agreement with XRD measurements. Present result indicates that nanophase Cu_3SbSe_4 are successfully incorporated in BiSbTe matrix, forming (Cu_3SbSe_4)/BiSbTe bulk nanocomposites. Fig. 3**(a)** gives the low magnification bright-field TEM image of Cu_3SbSe_4/BiSbTe, which shows that there are Cu_3SbSe_4 nanoparticles embedded in the BiSbTe matrix. Fig. 3**(b)** shows the lattice image (corresponding to the rectangle area in Fig. 3**(a)**) of BiSbTe matrix (lower-right), Cu_3SbSe_4 inclusion (upper-left), and a typical phase boundary (between the matrix and the dispersed phase), as shown by the two arrows.

The thermoelectric properties (ρ and S) of composites $f(Cu_3SbSe_4)$/BiSbTe (f = 0, 1, 2, and 3 vol.%) are shown in Figure 4 (the corresponding data of nanocrystalline (NC) BiSbTe bulk samples reported by Poudel *et al.*[11] are also depicted there for comparison). It can be seen from Figure 4**(a)** that ρ for all the composite samples $f(Cu_3SbSe_4)$/BiSbTe (f = 0, 1, 2, and 3 vol.%) (samples $0^\#$, $1^\#$, $2^\#$ and $3^\#$) increases with increasing temperature, indicating that they all exhibit a degenerate semiconductor behavior. On the other hand, ρ increases significantly with increasing f from 1 to 2 vol.% and then to 3 vol.%. However, ρ for sample $1^\#$ is smaller than that of sample $0^\#$ in whole temperature range investigated (ρ decreases from 0.69 to 0.63×10^{-5} Ωm at 304 K and from 1.30 to 1.11×10^{-5} Ωm at 490 K as f increases from 0 to 1 vol.%, for instance). Moreover, It is found that the slopes ($d\rho/dT$) of the ρ-T curves for samples with different f as well as NC BiSbTe differ obviously,[11] which are 3.34×10^{-8}, 2.61×10^{-8}, 4.12×10^{-8} and 4.36×10^{-8} Ω.m/K for f = 0, 1, 2 and 3 vol.%, respectively. Specially, it is noted that the $d\rho/dT$ for the sample $1^\#$ is obviously smaller than that of sample $0^\#$, which could involve significant scattering mechanism (see following discussion). Similar phenomena can be found in other material systems, such as $(Bi_2Sb_3)_{0.2}(Sb_2Te_3)_{0.8}$/α-$SiO_2$,[12] $Bi_{0.5}Sb_{1.5}Te_3/C_{60}$,[13] and β-$Zn_4Sb_3/Cu_3SbSe_4$[14] nanocomposites.

The temperature dependences of S are shown in Figure 4**(b)**. S values for all of the samples are positive, indicating that they belong to p-type semiconductors. The temperature behaviors of S for the sample $0^\#$ and NC BiSbTe are similar: S increases first with increasing temperature at T<~450 K.[11] Then it decreases with

further increase in temperature, which can be ascribed to the excitation of minority carriers (i.e. electrons) at high temperatures.[15] In contrast, *S* values of the composite samples with *f* = 1, 2 and 3 vol.% increase almost monotonically with temperature in the whole temperature range investigated here. In addition, *S* decreases obviously with increasing nanoinclusion content *f* (except *f* = 3 vol.%).

In order to understand better the behavior of ρ and S, carrier concentrations *p* for all the samples are determined at room temperature, as listed in Table 1. One can see that *p* increase from 4.52×10^{19} cm^{-3} to 5.50×10^{19} cm^{-3}, 7.41×10^{19} cm^{-3} and 8.98×10^{19} cm^{-3}, as *f* increase from 0 to 1 vol.%, 2 vol.% and 3 vol.%, respectively. Therefore, the decrease in ρ of sample 1# results largely from the increase in *p* due to the relation $\rho=(pe\mu)^{-1}$. In contrast, that ρ of samples 2# and 3# are larger than that of sample 1#can be attributed to the substantial decline of μ caused by the enhanced interface scattering. On the other hand, the thermopower of a degenerate semiconductor can be expressed by Mott formula:[16]

$$S = \frac{\pi^2 k_B{}^2 T}{3q}\left(\frac{\partial \ln(\sigma(E))}{\partial E}\right)_{E=E_f}$$

$$= \frac{\pi^2 k_B{}^2 T}{3q}\left[\frac{1}{p}\frac{\partial p(E)}{\partial E} + \frac{\partial \mu(E)}{\partial E}\right]_{E=E_f} \quad (1)$$

where *q*, k_B, E_f are the carrier charge, the Boltzmann constant, and the Fermi energy, respectively. Formula (1) indicates that *S* decreases with increasing *p* which can explain qualitatively why *S* of composite samples decrease with increasing *f*.

As mentioned above, the slopes of the ρ-*T* curves are different among the samples. Especially the slope of sample 1# is smaller than that of sample 0#. We assume here that *p* do not change substantially (which is true for a degenerate semiconductor at the temperatures below intrinsic excitation[17,18]) in the temperature range (300 K<T<450 K) investigated here. Then total μ_T can be estimated from values of ρ at different temperatures *T*, as shown in Figure 5**(a)**. If we assume that the scattering events are independent with each other, then one has:[19]

$$\frac{1}{\mu_T} = \frac{1}{\mu_m} + \frac{1}{\mu_{in}} \quad (2)$$

where μ_T, μ_m and μ_{in} are the total carrier mobility of the composite samples, the mobility of the matrix and the mobility being related to scattering of interface potentials. Based on the experimental data, one can extract μ_{in} by using formula (2), as given in Figure 5**(b)**. It can be seen that μ_{in} of sample 1# increases with increasing temperature, while μ_{in} of samples 2# and 3# decrease with increasing temperature. Similar to the scattering of grain boundary potentials, μ_{in} caused by interface scattering in nanocomposites can be approximately given by:[20,21]

$$\mu_{in} = Lq\left(\frac{1}{2\pi m_d^* k_B T}\right)^{1/2} \exp\left(-\frac{E_{Bp}}{k_B T}\right) \quad (3)$$

where *L* is the mean spacing between two adjacent potential barriers, and E_{Bp} is the height of the potential barrier at the interfaces. A logarithmic plot of $\mu_{in1}*T^{1/2}$ (μ_{in1} is μ_{in} of sample 1#) versus 1/T is shown in the inset of Figure 5**(b)**. From the slope the height of the potential barrier is extracted to be E_{Bp} = 67.1 meV. If we take $d\mu_{in}/dT = 0$, i.e.

$$\frac{d\mu_{in}}{dT} = Lq\left(\frac{1}{2\pi m_d^* k_B}\right)^{1/2} \frac{1}{T^{3/2}} \exp\left(-\frac{E_{Bp}}{k_B T}\right)\left(\frac{E_{Bp}}{k_B T} - \frac{1}{2}\right) = 0 \quad (4)$$

then we obtain a critical temperature $T_c = 2E_{Bp}/k_B$. Using E_{Bp} = 67.1 meV and $k_B = 1.38\times10^{-23}$ J/K, T_c = 1556 K is obtained, which means that when $T<T_c$, there exists $d\mu_{in1}/dT>0$. In our experiment, the temperature range investigated is 300-500 K; hence μ_{in1} increases with increasing temperature, which alleviates the increase rate in ρ of sample 1# (Figure 4**(a)**). With increasing *f* from 1 to 2 and then to 3 vol. %, *p* increase from 5.50×10^{19} cm^{-3} to 7.41×10^{19} cm^{-3} and then to 8.98×10^{19} cm^{-3}, and the depletion layer becomes narrow. As a result, E_{Bp} becomes smaller. Nonetheless, the scattering probabilities increase owing to substantial increase in scatterers, which cause the carriers to be scattered much stronger, as reflected by large decline of μ_{in} and the much enhanced EFE for samples 2# and 3# (as shown in Figure 6**(a)**). We estimate $E_{Bp}\leq12.9$ meV (When T_c= 300 K, E_{Bp} = 12.9 meV) and $d\mu_{in}/dT<0$ at 300-500 K, for μ_{in} of samples 2# and 3# decrease with increasing temperature as shown in Figure 5**(b)**, which cause ρ for samples 2# and 3# to increase more steeply (than that of sample 0#) with increasing temperature.

On the other hand, it is worthwhile to notice that *S* of sample 3# is slightly larger than that of sample 2# (as shown in Figure 4**(b)**), although *p* of the former is larger than that of the later (as shown in Table 1). This phenolmenon could be related to the EFE caused by the incorporation of Cu_3SbSe_4 nanoparticles. As we know, when two semiconductors (here BiSbTe and Cu_3SbSe_4) contact each other a (here p-p type) heterojunction potential (barrier) will form at the interfaces due to difference of the chemical potentials of the two semiconductors, which could cause energy-dependent scattering (or EFE) to occur,[22] as manifested by the increase of scattering parameter λ that is usually related to relaxation time τ by the relation: $\tau = \tau_0 E^{\lambda-1/2}$ (here E is the energy of carriers and τ_0 is energy-independent constant). By using a single parabolic band model, the density of state effective mass m_d^* and *S* can be expressed as:[23]

$$m_d^* = \frac{h^2}{2k_B T}\left(\frac{p}{4\pi F_{\frac{1}{2}}(\xi_F)}\right)^{\frac{2}{3}} \quad (5)$$

$$S = \frac{k_B}{e}\left[\frac{(\lambda+2)F_{\lambda+1}(\xi_F)}{(\lambda+1)F_\lambda(\xi_F)} - \xi_F\right] \quad (6)$$

with Fermi integral of order i

$$F_i(\xi_F) = \int_0^\infty \frac{x^i}{1+e^{(x-\xi_F)}}dx \quad (7)$$

where h and ξ_F are the Planck constant and the reduced Fermi level $F_f/(k_BT)$, respectively. Here, we assume that acoustic scattering is dominant in BiSbTe (i.e. λ=0 for sample 0#), and one obtains m_d^* = 1.38m_e (T = 300 K) and m_d^* = 1.22m_e (T = 443 K) (where m_e is the free electron mass) for sample 0#. Moreover, by assuming that the density of state effective mass do not change in different samples at the corresponding temperatures then one can calculate λ for samples 1#, 2# and 3# at T = 300 K and 443 K, respectively, as shown in Table 1. One can see that λ increases with increasing Cu_3SbSe_4 content. This increase of λ leads to ~3, ~7 and ~18 μV/K rise at 300 K and ~3, ~15 and ~26 μV/K rise at T = 443 K in S for samples 1#, 2# and 3#, respectively, as shown in Figure 6**(a)**, where the two lines are the Pisarenko relation of BiSbTe at T = 300 K and 443 K, respectively, which shows the dependence of S on p calculated by using formulae (5) and (6).

Moreover, another interesting phenomenon is that although S for sample 0# (and NC BiSbTe) declines at T>~450 K due to excitation of minorities, S for the composite samples 1#, 2# and 3# do not show decrease up to 500 K (the highest temperature investigated here). This result suggests that the introduced heterojunction potential barriers scatter electrons more strongly than holes. Since in the case of mixing conduction S can be written as following:[24]

$$S_T = \frac{\sigma_p S_p + \sigma_n S_n}{\sigma_p + \sigma_n} \quad (8)$$

where the subscript T, p and n represent total (hole and electronic conduction), hole conduction and electronic conduction, respectively. If electrons are scattered more strongly than holes, σ_n (or μ_n) will become negligibly small, and the term $|\sigma_n S_n|$ (S_n<0) in formula (8) can be neglected as compared to $\sigma_p S_p$. Then formula (8) becomes $S_T \approx S_p$, which explains why S of samples 1#, 2# and 3# monotonically increases with increasing temperature. In other words, the introduced heterojunction potential barriers have an asymmetric shape (i.e. the barrier height E_{Bn} for electrons is much higher than E_{Bp} for holes) as depicted schematically in Figure 6**(b)**.

Figure 7 shows PF of $f(Cu_3SbSe_4)$/BiSbTe as functions of temperature. One can see that PF of the composite samples increases slightly at the beginning; then PF decreases with further increasing temperature. Although PF of all the heavily incorporated samples (f = 2, and 3 vol.%) is smaller than that of the sample 0#, the PF of the lightly incorporated sample with f= 1 vol.% enhances obviously at T>~428 K, reaching 37 μW/(cm·K^2), which is ~5% larger than that of sample 0# and ~48% larger than that of NC BiSbTe.[11] This enhancement of PF for sample 1# at T>~428 K comes from increased both μ_{in} and S at elevated temperatures, which originates comprehensively from contributions of interface potentials: scattering with proper potential barriers for holes, asymmetric scattering to carriers (stronger scattering to electrons than to holes) and enhanced EFE.

The results of the specific heat, C_p, determined by DSC for BiSbTe and Cu_3SbSe_4 from 300 K to 500 K are shown in Fig. 8**(a)**. One can see that the values of C_p for BiSbTe range from 0.185 to 0.221 Jg^{-1}K^{-1}, while the values of C_p for Cu_3SbSe_4 range from 0.303 to 0.357 Jg^{-1}K^{-1}. Due to the small changes for the values of C_p in the temperature range from 300 K to 500 K, the average value of C_p is set here, i.e. C_p for BiSbTe is 0.20 Jg^{-1}K^{-1} and C_p for Cu_3SbSe_4 is 0.33 Jg^{-1}K^{-1}. For the composite sample, C_p can be determined by the rule of mixture:

$$C_{p_c} = (1-\chi)C_{p1} + \chi C_{p2} \quad (9)$$

with the mass fraction

$$\chi = \frac{f}{(1-f)\eta + f} \quad (10)$$

where C_{Pc}, C_{P1}, and C_{P1} are the specific heat for the composite sample, BiSbTe and Cu_3SbSe_4, respectively, and $\eta = d_1/d_2$, where d_1 and d_2 are the theoretical density of BiSbTe and Cu_3SbSe_4. Then we obtain the values of C_p for the composite samples 1#, 2# and 3#, which are almost the same as the C_p for BiSbTe matrix (due to small content of the nanoinclusions) and equal to 0.20 Jg^{-1}K^{-1}. The total thermal conductivity κ for all the samples, which is calculated from the measured thermal diffusivity D, specific heat C_p, and density d, is given in Figure 8**(b)** as a function of temperature. One can see that κ for all the composite samples (f>0) is smaller than that of sample 0# in the whole temperature range investigated here. Moreover, κ decreases monotonically with the increasing Cu_3SbSe_4 content f (except for the sample 3#). For instance, at 420 K, κ decreases from 1.3 to 1.1, 0.9 and then 1.0 μW/(cm·K^2) as f increase from 0 to 1, 2 and 3 vol.%. In addition, as compared to that of NC BiSbTe,[11] κ of all the composite samples decrease much faster with increasing temperature and becomes smaller at high temperature range (see Figure 8**(b)**). The total thermal conductivity κ consists of lattice thermal conductivity κ_L and the carrier thermal conductivity κ_c, i.e. $\kappa = \kappa_L + \kappa_c$, where κ_c can be estimated by the Wiedemann-Franz relation ($\kappa_c = LT/\rho$), in which the Lorenz number L is estimated using formula (10) with the assumption of transport dominated by acoustic scattering and a single parabolic band.[25]

$$L = (\frac{k_B}{e})^2 \frac{3F_0(\xi_F)F_2(\xi_F) - 4F_1(\xi_F)^2}{F_0(\xi_F)^2} \quad (11)$$

The obtained values of L are 1.68–1.81 × 10^{-8} V^2K^{-2}, as listed in Table 1. As shown in the inset of Figure 8**(b)**, the incorporation of 1 vol.% nanophase Cu_3SbSe_4 leads to ~50% reduction of κ_L as compared to that of sample 0#. According to Callaway mode, the lattice thermal conductivity κ_L can be expressed as:[26]

$$\kappa_L = \frac{4\pi k_B{}^4 T^3}{vh^3}\int_0^{\frac{\theta_D}{T}} \tau(\xi)\frac{\xi^4 e^\xi}{(e^\xi - 1)^2}d\xi \quad (12)$$

where h, θ_D, v, ξ and τ are plank constant, Debye temperature, phonon velocity, usual dimensionless variable and phonon relaxation time, respectively. Moreover, according to Matthiessen's rule, τ is mainly related to scattering from multiple scattering centers in the materials and can be written as:

$$\tau^{-1} = \tau_{PD}^{-1} + \tau_{NP}^{-1} + \tau_{P-P}^{-1} + \tau_{IF}^{-1} \quad (13)$$

where τ_{PD}, τ_{NP}, $\tau_{p\text{-}p}$ and τ_{IF} are the relaxation times correspond to scattering from point defect, nanoinclusions, phonon-phonon interactions and interfaces, respectively. Obviously, the reduction of κ_L in the composite samples 1#, 2# and 3# should be attributed to the additional phonon scattering from nanoinclusion (τ_{NP}) and the formed phase boundaries (τ_{IF}). However, we notice that with increasing f from 1 to 2 and 3 vol.%, κ_L rises instead of continuing falling, which could be caused by the inherent large lattice thermal conductivity κ_L of Cu_3SbSe_4,[27] which means that large proportion of its existence will inevitably lead to the increase in the overall κ_L of the composite system.

Figure 9 shows ZT for all the samples. One can see that ZT of sample 1# is larger than unit in the whole temperature range and even larger than that of NC BiSbTe at T>~375 K,[11] reaching 1.6 at 476K, which is ~22% larger than that of sample 0# (ZT_{max} = 1.3 at 418 K) and ~15% larger than that of NC BiSbTe (ZT_{max} = 1.4 at 373 K).[11] Clearly, such excellent thermoelectric performance result from both increased PF and reduced κ_L through interface scattering of both carriers and phonons. With such ZT characteristics, the present composite material system is attractive for power generation applications.

4. Conclusions

In summary, the incorporation of 1vol.% nano-Cu_3SbSe_4 particles into BiSbTe matrix can concurrently result in ~5% increase in PF and ~50% reduction of κ_L at 467 K. The increases in PF result from both alleviated reduction of carrier mobility and enhanced EFE at elevated temperatures due to carrier scattering at interface potential barriers in the composite system; while the reduction of κ_L in the composite samples is attributed to the enhanced phonon scattering at dispersed nanoparticles and the phase boundaries. Owing to increased PF and reduced κ_L, ZT = 1.6 is achieved at 476 K in the composite system with 1 vol.% of Cu_3SbSe_4. Present study demonstrates that the thermoelectric performance of BiSbTe can be effectively improved by incorporating proper amount of nanophase Cu_3SbSe_4.

Acknowledgements

Financial support from National Natural Science Foundation of China (Nos. 1374306, 50972146, 10904144, 11174292, 51101150, and 51202252) was gratefully acknowledged.

References

1. L. E. Bell, *Science*, 2008, **321**, 1457.
2. J. P. Heremans, V. Jovovic, E. S. Toberer, A. Saramat, K. Kurosaki, A. Charoenphakdee, S. Yamanaka, G. J. Snyder, *Science*, 2008, **321**, 554.
3. J. Zhang, X. Y. Qin, D. Li, *J. Mater. Chem. A*, 2014, **2**, 2891.
4. K. F. Hsu, S. Loo, F. Guo, W. Chen, J. S. Dyck, C. Uher, T. Hogan, E. K. Polychroniadis, M. G. Kanatzidis, *Science*, 2004, **303**, 818.
5. P. F. Poudeu, J. D'Angelo, A. D. Downey, *Angewandte Chemie*, 2006, **45**, 3835.
6. X. H. Yang, X. Y. Qin, *Appl. Phys. Lett*, 2010, **97**, 192101.
7. J. Heremans, C. Thrush, D. Morelli, *Phys. Rev. B*, 2004, **70**, 115334.
8. J. P. Heremans, C. M. Thrush, D. T. Morelli, *J. Appl. Phys*, 2005, **98**, 063703.
9. W. Xie, J. He, H. J.Kang, *Nano. Lett*, 2010, **10**, 3283.
10. T. R. Wei, H. Wang, Z. M. Gibbs, C. F. Wu, G. J. Snyder, J. F. Li, *J. Mater. Chem. A*, 2014, **2**, 13527.
11. B. Poudel, Q. Hao, Y. Ma, *Science*, 2008, **320**, 634.
12. Y. C. Dou, X.Y. Qin, D. Li, *J. Appl. Phys*, 2013, **114**, 044906.
13. V. D. Blank, S. G. Buga, V. A. Kulbachinskii, *Phys. Rev. B*, 2012, **86**, 075426.
14. T. H. Zou, X. Y. Qin, D. Li, *Appl. Phys. Lett*, 2014, **104**, 013904.
15. J. Zhang, X. Y. Qin, D. Li, *Elec. Mater. Lett*, 2015, **11**, 133.
16. Q. Q. Wang, X. Y. Qin, D. Li, *J. Appl. Phys*, 2013, **113**, 124901.
17. S. N. Girard, J. Q. He, X. Y. Zhou, D. Shoemaker, C. M. Jaworski, C. Uher, V. P. Dravid, J. P. Heremans, M. G. Kanatzidis, *J. Am. Chem. Soc*, 2011, **133**, 16588.
18. K. Biswas, J. Q. He, Q. C. Zhang, G. Y. Wang, C. Uher, V. P. Dravid, M. G. Kanatzidis, *Nature Chemistry*, 2011, **3**, 160.
19. J. Zhou, X. Li, G. Chen, R. Yang, *Phys. Rev. B*, 2010, 82, 115308.
20. J. Y. W. Seto, *J. Appl. Phys*, 1975, **46**, 5247.
21. J. Martin, L. Wang, L. Chen, G. Nolas, *Phys. Rev. B*, 2009, **79**, 115311.
22. Y. H. Yang, X. Y. Qin, *J. Appl. Phys*, 2011, **110**, 124308.
23. T. H. Zou, X. Y. Qin, D. Li, *J. Appl. Phys*, 2014, **115**, 053710.
24. D. Li, X. Y. Qin, *J. Appl. Phys*, 2006, **100**, 023713.
25. E. S. Toberer, P. Rauwel, S. Gariel, J. Tafto, G. J. Snyder, *J. Mater. Chem*, 2010, **20**, 9877.
26. Y. B. Luo, J. Y. Yang, M. Liu, Y. Xiao, L. W. Fu, W. X. Li, D. Zhang, M. Y. Zhang, Y. D. Cheng, *J. Mater. Chem. A*, 2015, **3**, 1251.

27. D. Li, R. Li, X. Y. Qin, *Dalton transactions*, 2014, **43**,1888

Table 1

List of Hall mobility μ, carrier concentration p, , the relative density d_r and the Lorenz number L at room temperature and scattering parameter λ at 300 K and 443 K for $f(Cu_3SbSe_4)$/BiSbTe nanocomposite samples (f = 0, 1, 2 and 3 vol.%).

f(vol.%)	$\mu(cm^2V^{-1}s^{-1})$[a]	p $(10^{19}cm^{-3})$[b]	λ_{300K}[c]	λ_{443K}[c]	$d_r(\%)$[d]	$L(10^{-8}V^2K^{-2})$[e]
0	201.7	4.52	0	0	94	1.68
1	180.4	5.50	0.04	0.62	95	1.71
2	90.6	7.41	0.11	0.76	94	1.77
3	53.1	8.98	0.25	0.96	94	1.81

[a] μ is Hall mobility.

[b] p is carrier concentration.

[c] λ is scattering parameter.

[d] d_r is relative density, defined as $d_r = d/d_0$, where d is measured density and d_0(= 6.76g/cm^3) is theoretical density of BiSbTe. For composite samples $f(Cu_3SbSe_4)$/BiSbTe, its theoretical density is modified as: $d_0 = (1-f)d_1+fd_2$, here $d_1 = d_0$ for BiSbTe and d_2(= 5.86g/cm^3) is theoretical density of Cu_3SbSe_4.

[e] L is the Lorenz number.

Figure caption

Figure 1. XRD patterns at room temperature of (a) BiSbTe, (b) Cu_3SbSe_4 and (c-e) f(Cu_3SbSe_4)/ BiSbTe (f = 1, 2 and 3 vol.%).

Figure 2. FE-SEM micrographs of **(a)** BiSbTe powders, **(b)** Cu_3SbSe_4 powders, **(c)** fracture surface of f(Cu_3SbSe_4)/BiSbTe bulk composite sample, **(d)** EDS pattern detected in the marked area in **(c)**.

Figure 3. (a) TEM bright-field image of Cu_3SbSe_4/BiSbTe shows the BiSbTe matrix and incorporated nanophase Cu_3SbSe_4 and **(b)** HRTEM image of the selected rectangle area in **(a)**.

Figure 4. Temperature dependences of **(a)** electrical resistivity and **(b)** Seebeck coefficient for composite samples f(Cu_3SbSe_4)/BiSbTe (f = 0, 1, 2 and 3 vol.%) and nanocrystalline BiSbTe bulk sample in Poudel's work.

Figure 5. Temperature dependences of **(a)** total carrier mobility μ_T and **(b)** carrier mobility that corresponds to the scattering of carriers at the interfaces μ_{in} for composite samples f(Cu_3SbSe_4)/BiSbTe (f = 0, 1, 2 and 3 vol.%). The inset of **(b)** is alogarithmic plot of μ_{in}*$T^{1/2}$ versus 1/T (300 K<T<450 K), and from the slope the height of the potential barrier is extracted to be E_B = 67.1 meV.

Figure 6. (a) Variation of Seebeck coefficient with carrier concentration for f(Cu_3SbSe_4)/BiSbTe (f = 0, 1, 2 and 3 vol.%) at 300 K and 443 K. The violet solid line is Pisarenko relation for BiSbTe at 300 K, and the pink dash dot line is at 443 K. **(b)** Cross sectional schematics of the energy bands for Cu_3SbSe_4 (band gap Eg_1)and BiSbTe matrix (band gap Eg_0) and p-p type interface potential barriers with an effective barrier height E_{Bp} and E_{Bn} formed from band bending (where Ec_0 and Ec_1 are the conduction band bottoms; Ev_0 and Ev_1 are the valence band tops and d_p is the grain size of Cu_3SbSe_4)

Figure 7. Temperature dependences of power factor for composite samples f(Cu_3SbSe_4)/BiSbTe (f = 0, 1, 2 and 3 vol.%) and nanocrystalline BiSbTe bulk sample in Poudel's work.

Figure 8. (a) Temperature dependences of the specific heat for BiSbTe and Cu_3SbSe_4. **(b)** Temperature dependences of total thermal conductivity (lattice thermal conductivity in the inset) for composite samples f(Cu_3SbSe_4)/BiSbTe (f = 0, 1, 2 and 3 vol.%) and nanocrystalline BiSbTe bulk sample in Poudel's work.

Figure 9. Temperature dependences of ZT for composite samples f(Cu_3SbSe_4)/BiSbTe (f = 0, 1, 2 and 3 vol.%) and nanocrystalline BiSbTe bulk sample in Poudel's work.

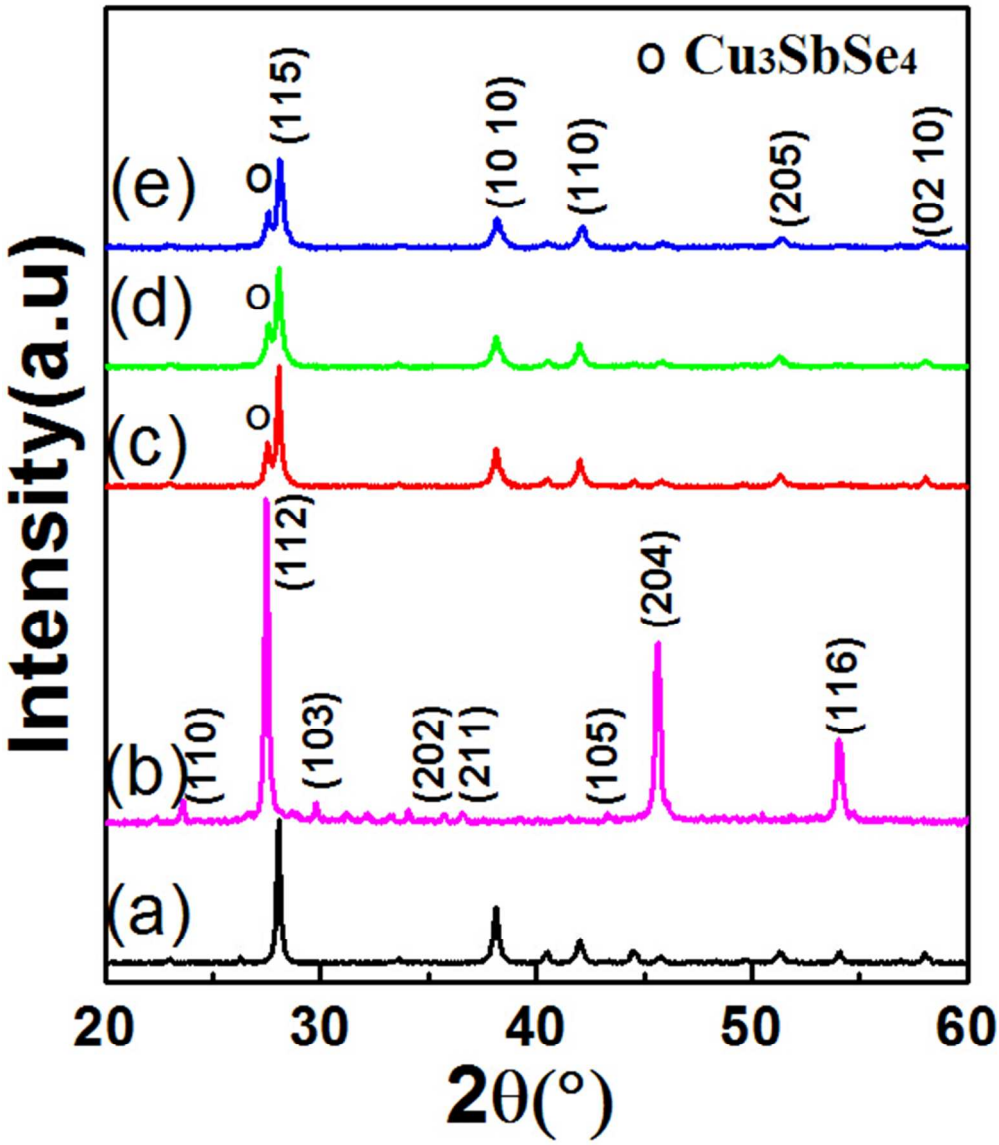

Fig-1
155x179mm (96 x 96 DPI)

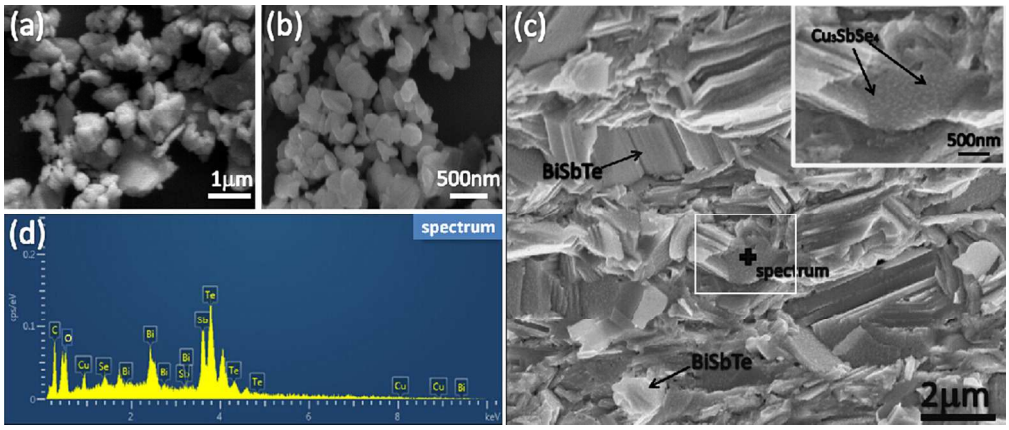

Fig-2
303x127mm (96 x 96 DPI)

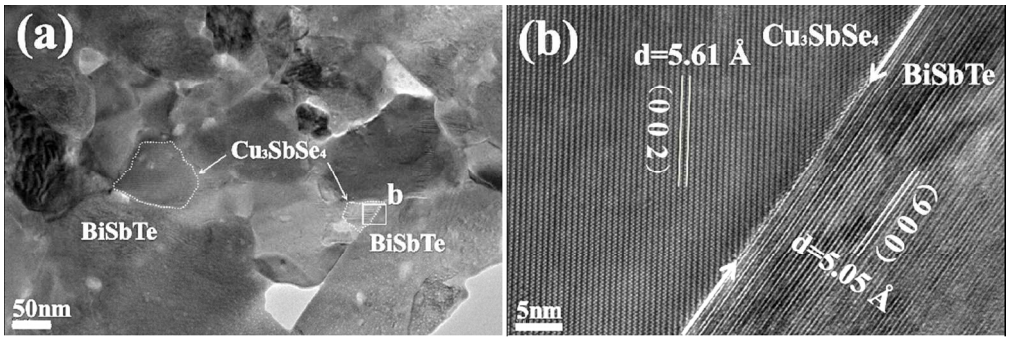

Fig-3
304x100mm (96 x 96 DPI)

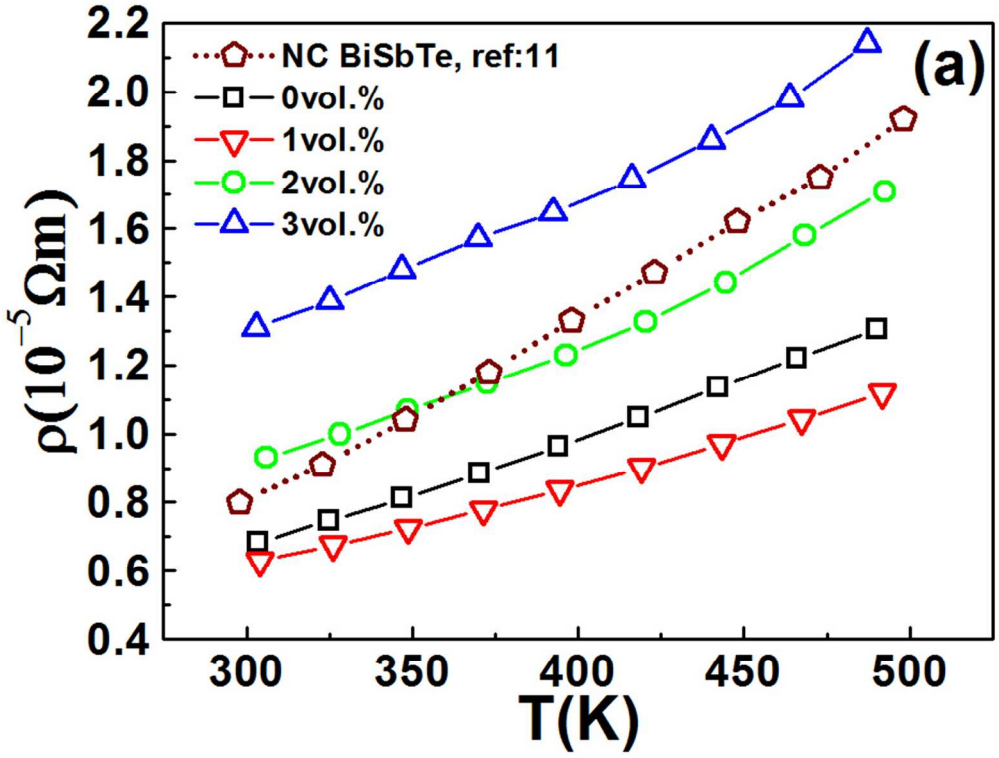

Fig-4(a)
246x186mm (96 x 96 DPI)

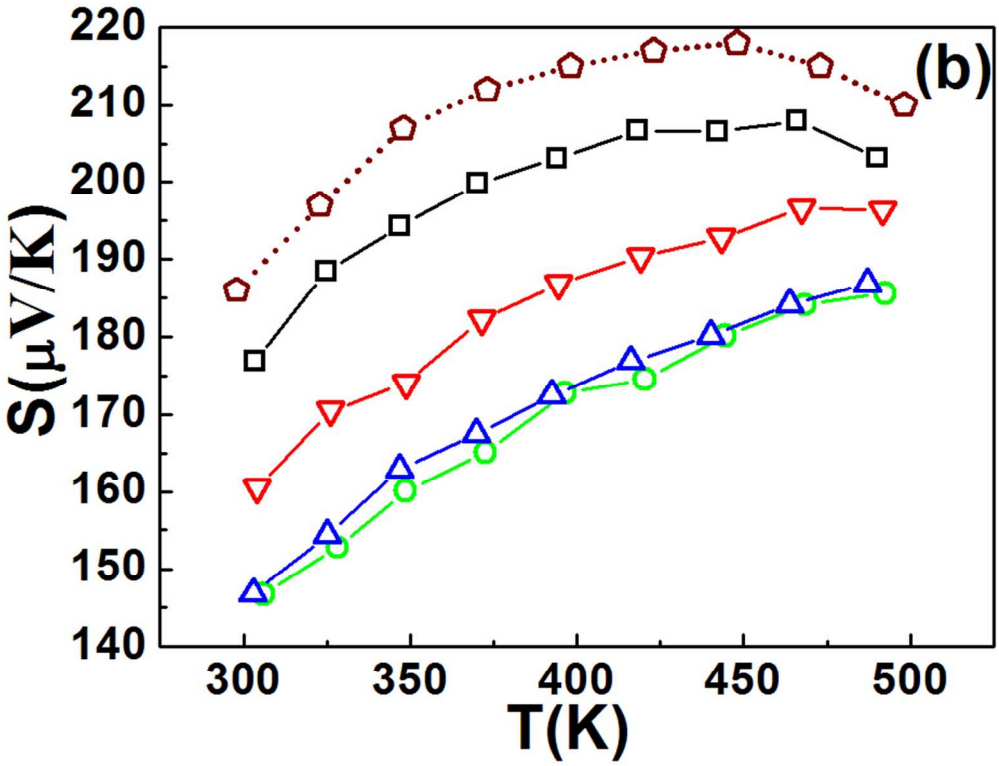

Fig-4(b)
245x186mm (96 x 96 DPI)

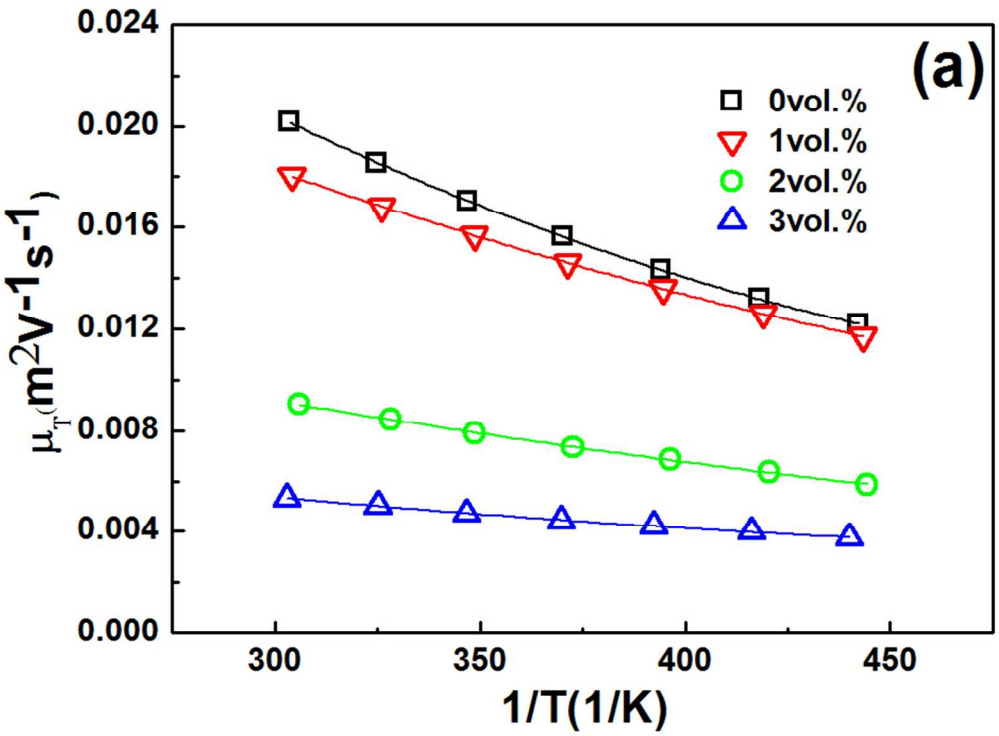

Fig-5(a)
249x182mm (96 x 96 DPI)

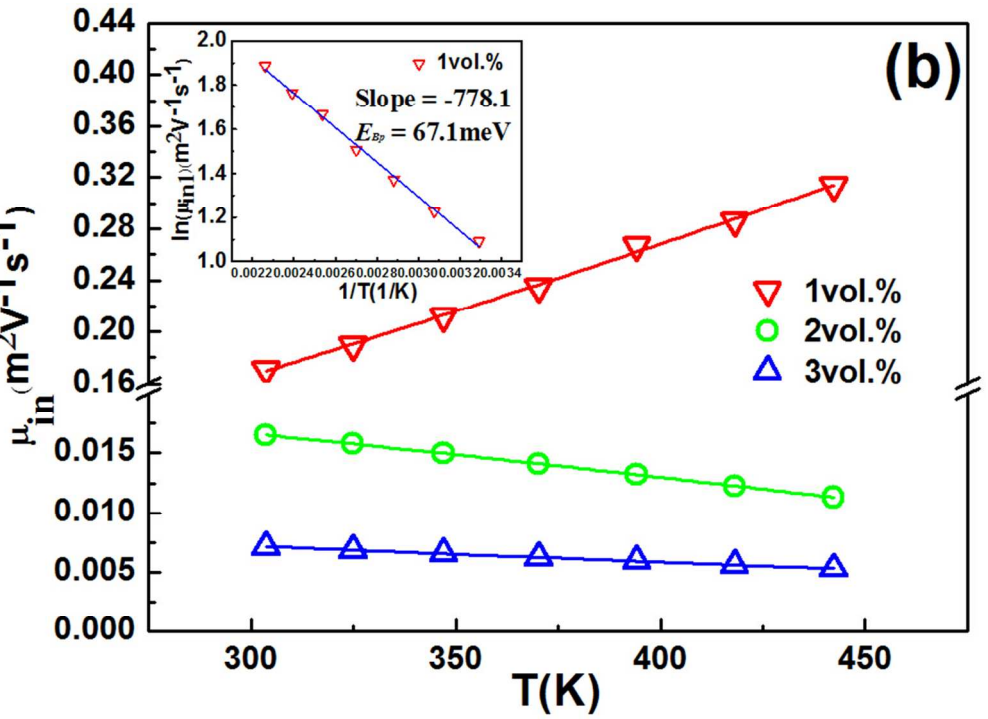

Fig-5(b)
249x178mm (96 x 96 DPI)

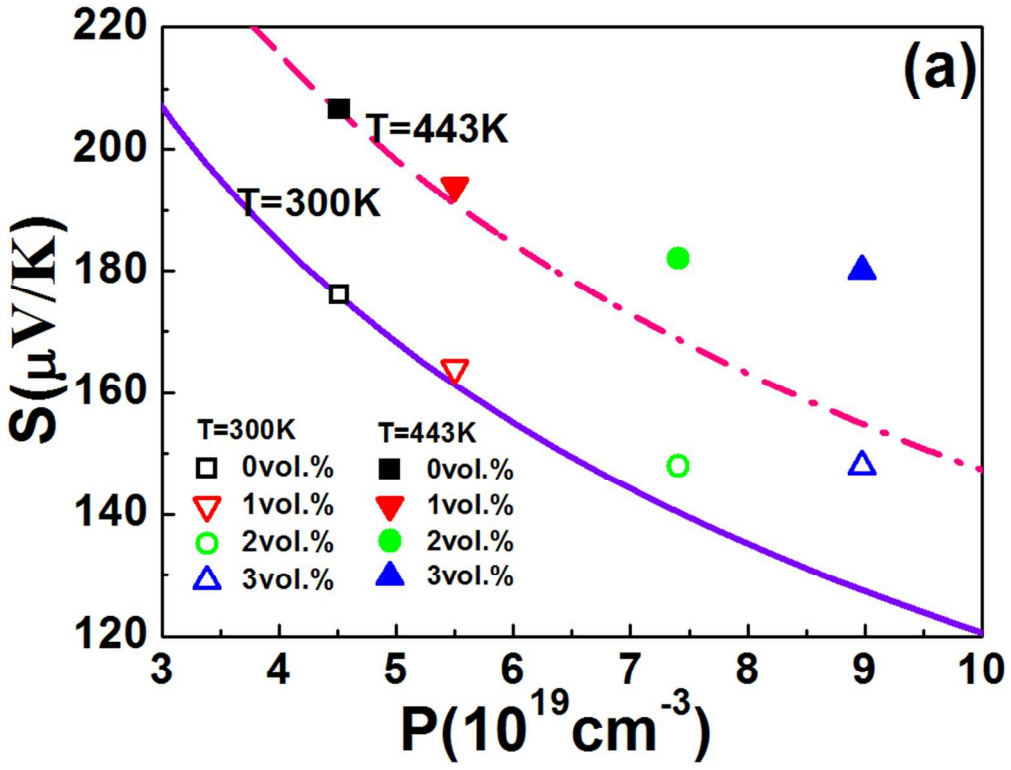

Fig-6(a)
249x189mm (96 x 96 DPI)

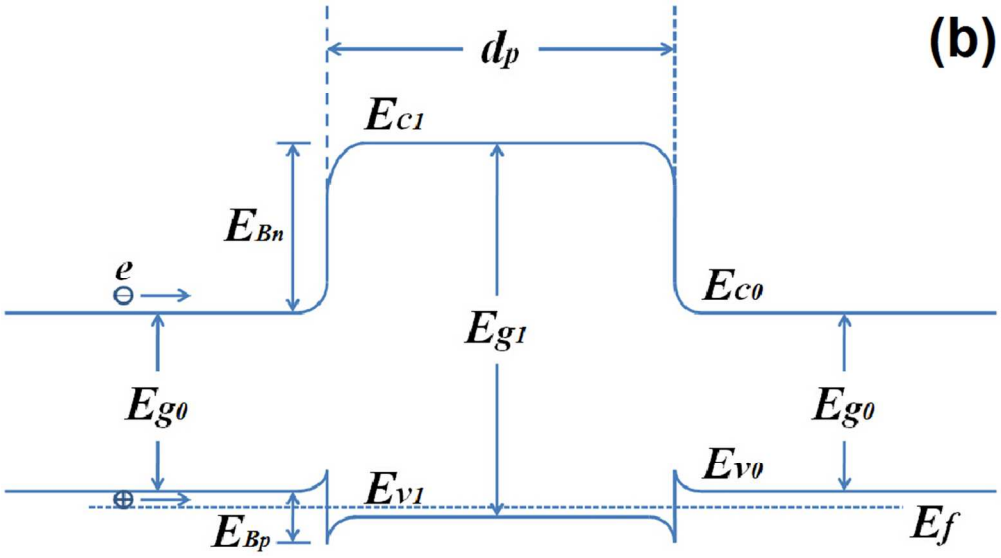

Fig-6(b)
285x158mm (96 x 96 DPI)

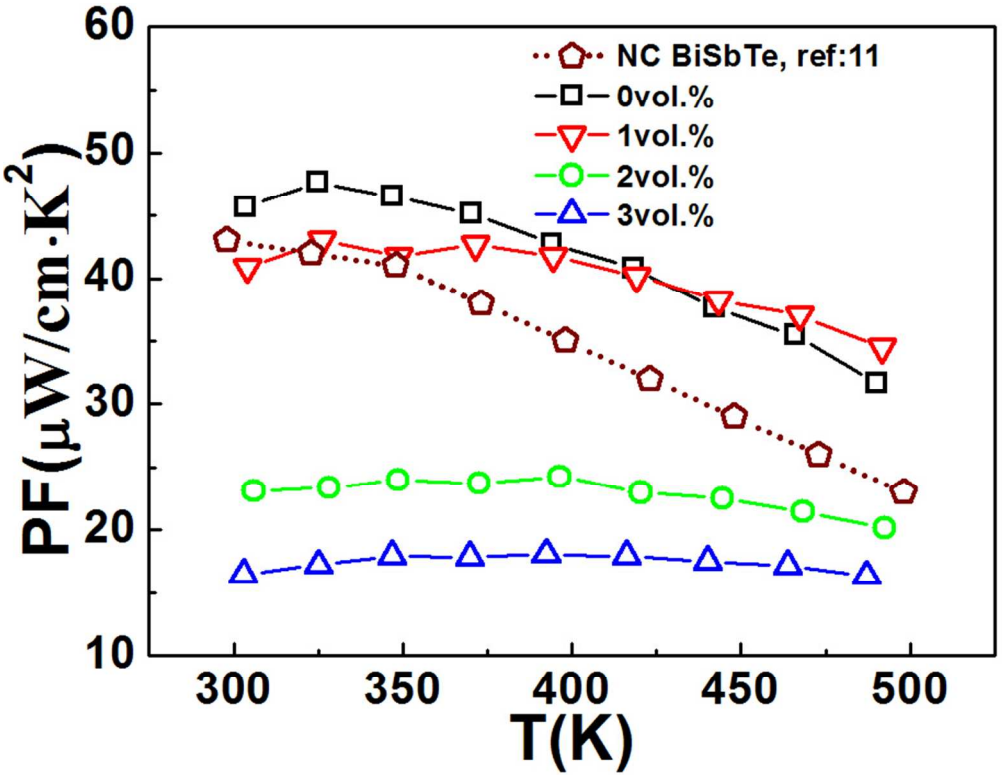

Fig-7
241x186mm (96 x 96 DPI)

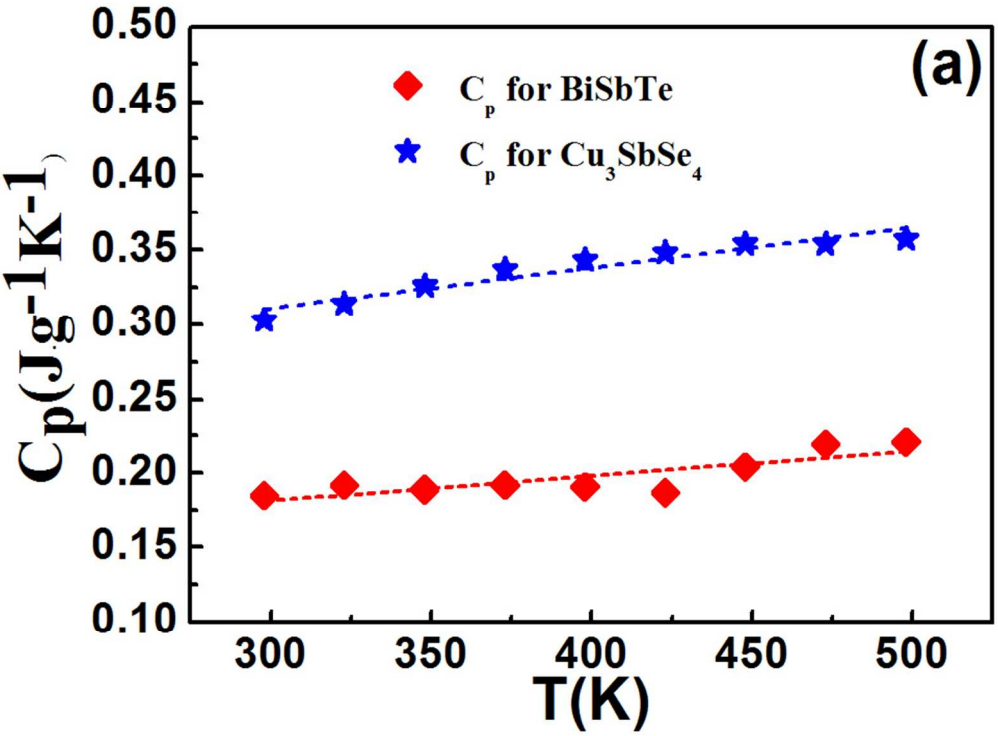

Fig-8(a)
255x186mm (96 x 96 DPI)

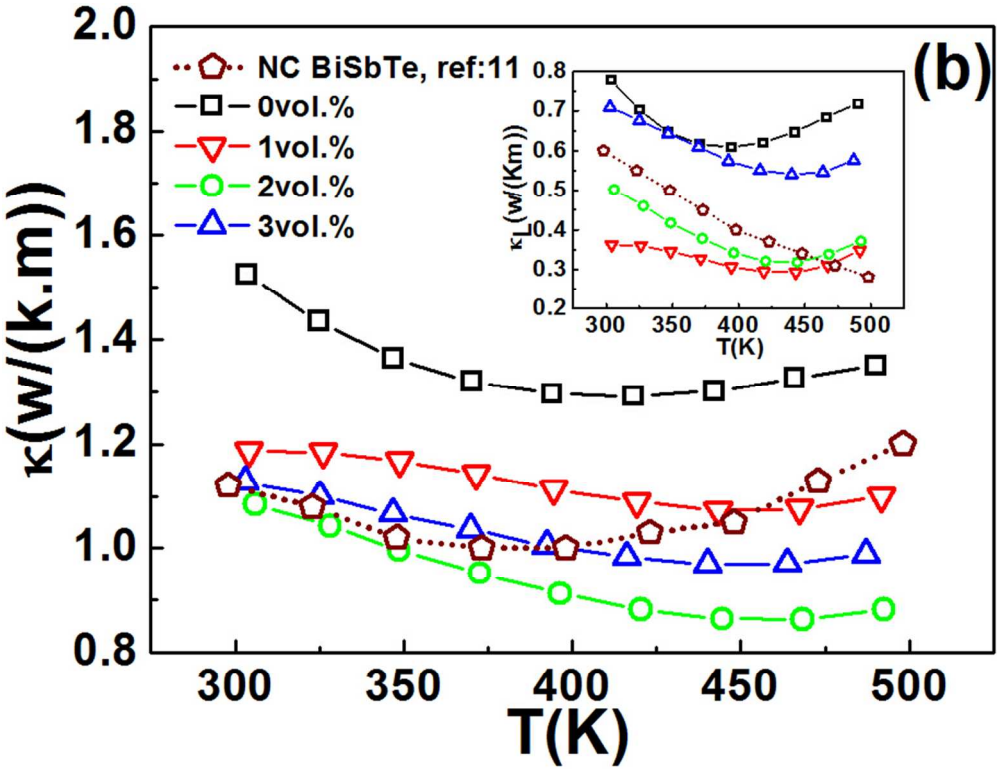

Fig-8(b)
242x185mm (96 x 96 DPI)

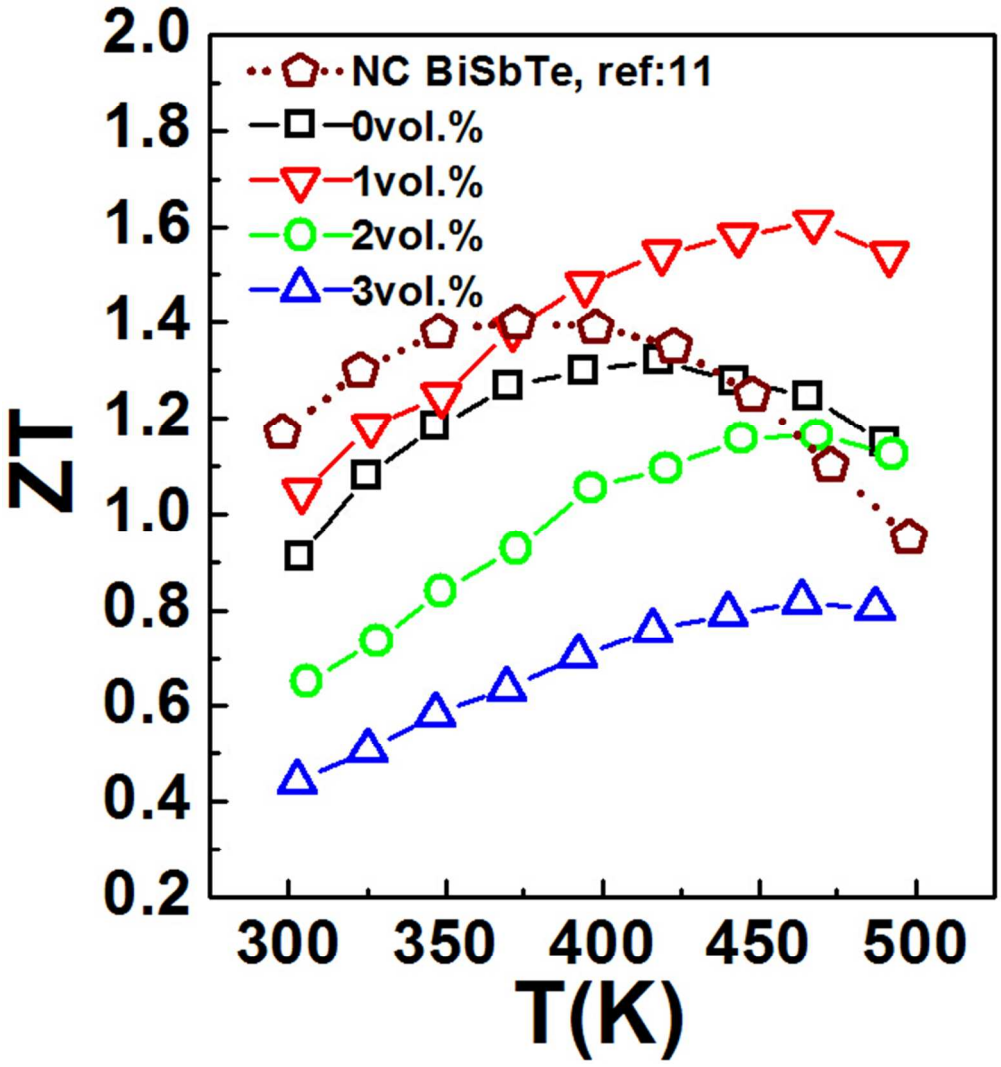

Fig-9
175x187mm (96 x 96 DPI)